

Calibration of Capacitance Probe Sensors using Electric Circuit Theory

T. J. Kelleners,* R. W. O. Soppe, D. A. Robinson, M. G. Schaap, J. E. Ayars, and T. H. Skaggs

ABSTRACT

Capacitance probe sensors are an attractive electromagnetic technique for estimating soil water content. There is concern, however, about the influence of soil salinity and soil temperature on the sensors. We present an electric circuit model that relates the sensor frequency to the permittivity of the medium and that is able to correct for dielectric losses due to ionic conductivity and relaxation. The circuit inductance L is optimized using sensor readings in a modified setup where ceramic capacitors replace the sensor's capacitance plates. The three other parameters in the model are optimized using sensor readings in a range of nonconductive media with different permittivities. The geometric factor for the plastic access tube g_p is higher than the geometric factor for the medium g_m , indicating that most of the electromagnetic field does not go beyond the access tube. The effect of ionic conductivity on the sensor readings is assessed by mixing salts in three of the media. The influence is profound. The sensor frequency decreases with increasing conductivity. The effect is most pronounced for the medium with the lowest permittivity. The circuit model is able to correct for the conductivity effect on the sensors. However, as the dielectric losses increase, the frequency becomes relatively insensitive to permittivity and small inaccuracies in the measured frequency or in the sensor constants result in large errors in the calculated permittivity. Calibration of the capacitance sensors can be simplified by fixing two of the constants and calculating the other two using sensor readings in air and water.

SOIL WATER CONTENT is a key factor in agriculture. Water content impacts crop growth directly, and also influences the fate of agricultural chemicals applied to soils. Estimation of soil water content, therefore, has received a lot of attention in the past. In the field, basically three methods are available: gravimetric techniques, nuclear techniques (e.g., neutron scattering), and electromagnetic techniques. Of these, electromagnetic techniques have become popular because they facilitate a rapid, safe, nondestructive, and easily automated estimation of soil water content.

Among the electromagnetic techniques, time domain reflectometry (TDR) is the most common method (e.g., Fellner-Felldeg, 1969; Topp et al., 1980; Baker and Allmaras, 1990; Heimovaara, 1994; Gardner et al., 2000; Noborio, 2001). However, the emergence of high qual-

ity, low-cost high frequency oscillators has led to increased interest in capacitance techniques (e.g., Dean et al., 1987; Evett and Steiner, 1995; Paltineanu and Starr, 1997). Capacitance probes are relatively inexpensive and easy to operate. Furthermore, the sensor geometry is very adaptable, facilitating the development of a variety of configurations (Robinson et al., 1998). However, capacitance probes are influenced by soil type and require calibration. Also, there is concern about the influence of soil salinity and soil temperature on capacitance sensors.

Several investigators have calibrated capacitance sensors for particular soil types (e.g., Bell et al., 1987; Evett and Steiner, 1995; Mead et al., 1995; Paltineanu and Starr, 1997; Morgan et al., 1999; Baumhardt et al., 2000). In these studies, the readout from the sensors (a frequency) is related directly to the water content of the soil. Generally, a scaled frequency is used to compensate for differences between sensors. From a theoretical standpoint, however, it must be realized that capacitance sensors actually react to the permittivity of the soil, which in turn is a function of the water content. Splitting the calibration into two stages, one in which frequency is related to permittivity, and one in which permittivity is related to soil water content, permits a more physically based calibration procedure.

A major advantage of the two-stage approach is that the relationship between permittivity and soil water content can be described by existing dielectric mixing models (e.g., Dobson et al., 1985; Dirksen and Dasberg, 1993; Friedman, 1998) or empirical models (e.g., Topp et al., 1980; Malicki et al., 1996). The relationship between frequency and permittivity, on the other hand, can be described with help of electric circuit theory as shown by Dean (1994) and Robinson et al. (1998). Electric circuit theory also makes it possible to account for the effect of dielectric losses due to ionic conductivity and relaxation on the sensor frequency reading. This implies that temperature effects on the sensor reading, which work primarily through an increase or decrease in ionic conductivity, can be accounted for as well.

In this work we develop an electric circuit model for capacitance probe sensors marketed as EnviroSCAN (Sentek Pty Ltd., Kent Town, South Australia). More specifically, the objectives of this study are (i) to determine the four sensor constants in the electric circuit model for the EnviroSCAN sensors, (ii) to demonstrate the effect of ionic conductivity on the sensor readings, (iii) to test the ability of the circuit model to correct for conductivity effects, and (iv) to develop a practical approach to calibrate the circuit model using only frequency readings in air and water.

T.J. Kelleners, D.A. Robinson, M.G. Schaap, and T.H. Skaggs, USDA-ARS, George E. Brown, Jr. Salinity Lab., 450 W. Big Springs Rd, Riverside, CA 92507; T.J. Kelleners, R.W.O. Soppe, and J.E. Ayars, USDA-ARS, Water Management Research Lab., 9611 S. Riverbend Ave., Parlier, CA 93648; R.W.O. Soppe, currently at Alterra-ILRI, P.O. Box 47, 6700 AA Wageningen, The Netherlands; D.A. Robinson, currently at the Dep. of Plants, Soils, and Biometeorology, Utah State Univ., Logan, UT 84322-4820. The mention of trade or manufacturer names is made for information only and does not imply an endorsement, recommendation, or exclusion by the USDA-ARS. Received 18 Nov. 2002. *Corresponding author (tkelleners@ussl.ars.usda.gov).

Published in Soil Sci. Soc. Am. J. 68:430–439 (2004).
© Soil Science Society of America
677 S. Segoe Rd., Madison, WI 53711 USA

Abbreviations: TDR, time domain reflectometry.

THEORY

The capacitance as observed by a capacitance probe sensor can be related to the relative permittivity of a medium through:

$$C = g\epsilon_r\epsilon_0 \quad [1]$$

where C is the capacitance ($L^{-2} T^4 M^{-1} I^2$) expressed in Farad (F), g is a geometric factor (L) associated with the electric field penetrating the measured media, ϵ_r is the relative permittivity (-) and ϵ_0 is the permittivity in vacuum ($L^{-3} T^4 M^{-1} I^2$) ($= 8.8542 \times 10^{-12} \text{ F m}^{-1}$).

The capacitance can be assessed by measuring the resonant frequency in an oscillator circuit:

$$F = \frac{1}{2\pi\sqrt{LC_t}} \quad [2]$$

where F is the resonant frequency (T^{-1}) expressed in Hertz (Hz), L is the total circuit inductance ($L^2 T^{-2} M I^{-2}$) expressed in Henry (H), and C_t is the total circuit capacitance.

It is assumed that the oscillator circuit of the capacitance probe sensors used in this study can be represented by the equivalent electric circuit shown in Fig. 1. The figure shows that the total circuit capacitance is made up of three components, which act both in parallel and in series:

$$C_t = C_s + \frac{C_p C}{C_p + C} \quad [3]$$

where C is the capacitance of the medium, C_p is the capacitance of the plastic access tube surrounding the sensor, and C_s is the capacitance due to stray electric fields. Both C and C_p can be written as a function of relative permittivity so that $C = g_m\epsilon_{r,m}\epsilon_0$ and $C_p = g_p\epsilon_{r,p}\epsilon_0$, where the subscript m denotes the medium and the subscript p denotes the plastic access tube.

Inserting Eq. [3] into [2] results in:

$$F = \frac{1}{2\pi\sqrt{L\left(C_s + \frac{C_p C}{C_p + C}\right)}} \quad [4]$$

Equation [4] is valid if the medium behaves as a nonlossy dielectric. In reality, losses due to relaxation and in some circumstances due to ionic conductivity result in lossy dielectrics. The relative permittivity of the medium should then be represented by a complex quantity ϵ_r^* that has a real part ϵ_r' describing energy storage and an imaginary part ϵ_r'' describing losses:

$$\epsilon_r^* = \epsilon_r' - j\epsilon_r'' \quad [5]$$

where $j^2 = -1$. Hereafter, ϵ_r' is referred to as ϵ_r . The ϵ_r'' term in Eq. [5] is the sum of a conductivity term and a relaxation term (Kraus, 1984):

$$\epsilon_r'' = \frac{\sigma}{\omega\epsilon_0} + \epsilon_{r,rel}'' \quad [6]$$

where σ is the ionic conductivity ($L^{-3} T^3 M^{-1} I^2$), expressed in $S m^{-1}$, ω is the angular frequency (T^{-1}) ($= 2\pi F$) and $\epsilon_{r,rel}''$ is the loss factor (-) due to relaxation.

The medium capacitance C is now also a complex quantity:

$$C^* = C' - j\left(\frac{g_m\sigma}{\omega} + g_m\epsilon_{r,rel}''\epsilon_0\right) \quad [7]$$

where C^* is the complex medium capacitance and C' is the

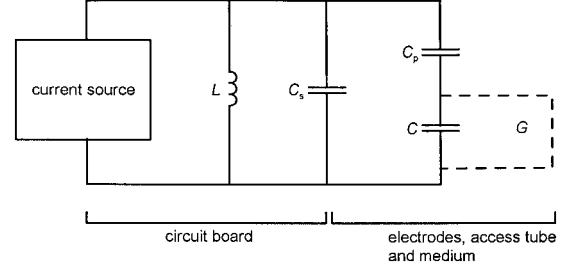


Fig. 1. Equivalent circuit for the capacitance probe sensor where L is the inductor, C is the capacitance of the medium, C_p is the capacitance of the plastic access tube, C_s is the stray capacitance and G is the energy loss due to relaxation and ionic conductivity.

real part of the medium capacitance (referred to as C in the remainder of this paper).

It is convenient to write Eq. [7] as:

$$j\omega C^* = j\omega C + G \quad [8]$$

where $G = g_m\sigma + g_m\omega\epsilon_{r,rel}''\epsilon_0$ (in Siemens).

To describe the behavior of the (parallel) oscillator circuit in lossy dielectrics, we calculate the admittance Y ($L^{-2} T^3 M^{-1} I^2$) of the circuit expressed in Ohm^{-1} . The appropriate equation for the circuit in Fig. 1 is:

$$Y = \frac{1}{Z} = \frac{1}{j\omega L} + j\omega C_s + \frac{j\omega C_p(j\omega C + G)}{j\omega C_p + j\omega C + G} \quad [9]$$

where Z is the impedance ($L^2 T^{-3} M I^{-2}$) of the circuit expressed in Ohm.

Separating the real and imaginary components gives:

$$Y = [-\omega^3 L C_p^2 G + j(\omega^2 C_A^2 + G^2 - \omega^4 C_s L C_A^2 - \omega^2 C_s L G^2 - \omega^4 L C_p C C_A - \omega^2 L C_p G^2)] / \omega L(-\omega^2 C_A^2 - G^2) \quad [10]$$

where $C_A = (C_p + C)$. At the resonance frequency for a parallel oscillator circuit, the current is in phase with the voltage (unity power factor). The circuit admittance is then a real quantity. Or, in other words, at the resonance frequency the imaginary part of Y is zero:

$$\omega^2 C_A^2 + G^2 - \omega^4 C_s L C_A^2 - \omega^2 C_s L G^2 - \omega^4 L C_p C C_A - \omega^2 L C_p G^2 = 0 \quad [11]$$

Equation [11] can be solved for the angular frequency ω or for the medium capacitance C using the quadratic formula. Solving for angular frequency requires that G be estimated directly. The G term cannot be calculated analytically using $G = g_m\sigma + g_m\omega\epsilon_{r,rel}''\epsilon_0$ because ω is not known a priori. On the other hand, when solving for medium capacitance, it should be realized that C is also included in C_A . Application of the quadratic formula to solve for C therefore requires some additional but straightforward algebraic operations. The resulting equations are given in the appendix.

MATERIALS AND METHODS

Two EnviroSCAN capacitance probes were used in this study. Probe 1 held 14 sensors while Probe 2 held 15 sensors. EnviroSCAN sensors consist of two brass rings (50.5-mm diameter and 25 mm high) mounted on a plastic sensor body and separated by a 12-mm plastic ring. The rings of the sensor form the plates of the capacitor. The sensors are designed to operate inside a PVC access tube. The frequency of oscillation depends on the permittivity of the media surrounding the tube. Sensitivity studies show that 90% of the sensor's response is

obtained from a zone that stretches from about 3 cm above and below the center of the plastic ring to about 3 cm in radial direction (starting from the access tube). More details about this particular type of capacitance sensor can be found in Paltineanu and Starr (1997).

Resonant frequency was measured in a variety of nonconductive dielectric media. We used air ($\epsilon_r = 1$), motor oil (≈ 2), corn (*Zea mays* L.) oil (≈ 3), brasso (a siliceous polishing powder suspended in an ammonium soap jelly and dispersed in petroleum distillates, used for polishing metals, ≈ 8), propanol (≈ 20), and deionized water (di-water ≈ 80). In addition, three mixtures of propanol and di-water (ϵ_r range 25–32) and five mixtures of di-water and sugar (range 45–75) were used. This resulted in 14 different media with a wide range of permittivities. The effect of ionic conductivity on the resonant frequency was measured by mixing different amounts of KCl in three media, namely propanol-di-water, sugar-di-water, and di-water. The electrical conductivity of the solutions was measured with an Orion model 170 conductivity meter (Orion Research Inc., Boston, MA) and ranged from 0.000 to 0.296 S m⁻¹. The frequency-permittivity experiments were conducted in 20-L plastic buckets with the polyvinyl chloride (PVC) access tube located in the center (running through the bottom of the bucket). Readings were taken by moving the sensors one by one into the center of the access tube. Air temperature in the laboratory was maintained at 25°C. The temperature of the media ranged between 23 and 28°C.

The dielectric properties (ϵ_r and ϵ_r'') of all of the media were measured with a network analyzer (Hewlett-Packard model 8753B, Hewlett-Packard, Palo Alto, CA) using a dielectric probe (Hewlett-Packard 85070B, Hewlett-Packard, Palo Alto, CA). Network analyzers are used in electronics to determine the reflection and transmission characteristics of devices and networks using a broad bandwidth signal (frequencies between 300 KHz and 3 GHz). In the frequency domain the reflection measurements can be used directly to obtain the ϵ_r and ϵ_r'' permittivities of a material as a function of frequency (Heimovaara et al., 1996). Measurements were conducted by placing the probe (basically a coaxial ring) in 50-mL subsamples that were taken from the 20-L buckets. In the subsequent analysis of the nonconductive media it was assumed that $\sigma = 0$ so that ϵ_r'' equals $\epsilon_{r,rel}''$ (Eq. [6]). For the conductive media, $\epsilon_{r,rel}''$ was calculated by subtracting $\sigma/\omega\epsilon_0$ from ϵ_r'' .

To assess the value of the circuit inductance L for the sensors, the circuit board of Sensor 15 on Probe 2 was separated from the plastic sensor body with the brass rings. Single ceramic capacitors C_c ranging in value from 1×10^{-12} to 56×10^{-12} F were soldered onto the circuit board to replace the brass rings and to close the circuit. This eliminated C ($= g_m\epsilon_{r,m}\epsilon_0$) and C_p ($= g_p\epsilon_{r,p}\epsilon_0$) with the unknown geometric factors g_m and g_p from the electric circuit, reducing the unknown parameters in the circuit model to L and C_s . The resonant frequency was measured for each C_c . The appropriate equation for this simplified oscillator circuit is:

$$F = \frac{1}{2\pi\sqrt{L(C_s + C_c)}} \quad [12]$$

The unknown parameters L and C_s in Eq. [12] were determined by minimizing the sum of the squared deviations between measured and calculated resonant frequency. The minimization was accomplished using the FMINSEARCH function in Matlab (The Mathworks Inc., Natick, MA), which uses the simplex search method (Coleman et al., 1999). Different seed values were used in the minimization to check the uniqueness of the solution.

Subsequently, the 14 combinations of resonant frequency

and permittivity for the nonconductive media for each sensor were used to optimize C_s , g_m , and g_p for all sensors. During these optimizations the value of the inductance L was fixed to the value measured for Sensor 2.15. We did not fix the value of C_s because we anticipated that this value would alter in response to the change in the setup of the electric circuit. The optimization was done by solving Eq. [11] for C ($= g_m\epsilon_{r,m}\epsilon_0$) and minimizing the sum of the squared deviations between measured and calculated relative permittivity. The minimization was again accomplished using the FMINSEARCH function in Matlab. Different seed values were used in the minimization to check the uniqueness of the solution. During all calculations the relative permittivity of the PVC access tube, $\epsilon_{r,p}$ was assumed to be 3 (e.g., Von Hippel, 1954).

The described two-step approach for determining the sensor constants proved necessary because simultaneous optimization of all four unknowns in the circuit model using Eq. [11] did not result in unique parameter values. Ideally, we would have determined the inductance L for all the sensors individually. This however would involve damaging all 29 sensors, which was considered too costly.

RESULTS AND DISCUSSION

Circuit Inductance

The values for the inductance L and the stray capacitance C_s that result in the smallest sum of squares for Sensor 2.15 are 9.38×10^{-8} H and 4.52×10^{-12} F, respectively. The fit of the optimized frequency response (Eq. [12]) to the measured frequency response is shown in Fig. 2. The comparison is good ($R^2 = 0.997$). Note that the plotted values for C_c only range between 5×10^{-12} and 39×10^{-12} F, while the tested capacitors had values between 1×10^{-12} and 56×10^{-12} F. Capacitors of 1, 2, 4, and 56×10^{-12} F resulted in a “failure” warning from the probe’s data recording software because the circuit frequency was considered out of range (i.e., outside the range of frequencies as obtained when measuring in air and water).

The circuit inductance L should be equal to or higher than the inductance of the coil depicted in Fig. 1 (the difference being due to stray inductance associated with the circuit board tracks). The coil inductance, L_{coil} can be calculated as:

$$L_{coil} = \frac{\mu_r\mu_0 N^2 \pi r^2 K}{l} \quad [13]$$

where μ_r is the relative magnetic permeability ($= 1.0$ for air), μ_0 is the magnetic permeability in vacuum ($= 1.2566 \times 10^{-6}$ H m⁻¹), N is the number of turns in the coil ($= 7$), r is the radius of the coil, l is the length of the coil ($= 0.004$ m) and K is a constant depending upon the ratio of the diameter to the length (e.g., Terman, 1943).

The calculated value for L_{coil} is either 1.07×10^{-7} H (using $r = 0.00175$ m, the average of the inner and outer radius of the coil and $K = 0.72$) or 8.16×10^{-8} H (using $r = 0.0015$ m, the inner radius of the coil and $K = 0.75$). The first value applies to low-frequency circuits while the second value applies to high-frequency circuits where the current crowds toward the inside of the coil. The optimized circuit inductance of 9.38×10^{-8} H for

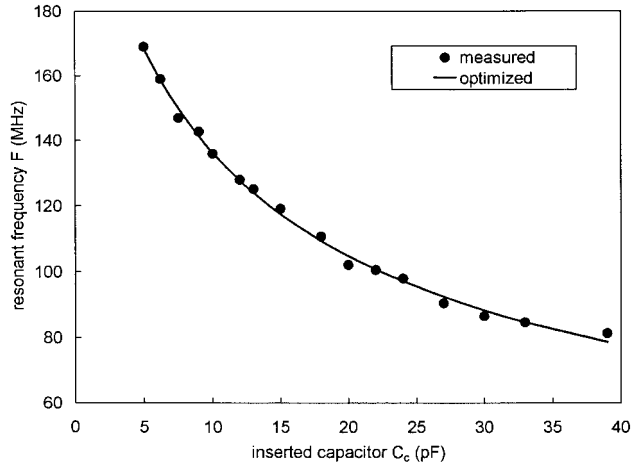


Fig. 2. Measured and optimized resonant frequency of Sensor 2.15 as a function of the inserted Capacitor C_c .

our (high-frequency) sensor is only slightly higher than the calculated L_{coil} value of 8.16×10^{-8} H. This indicates that the stray inductance in the circuit is small (on the order of 1×10^{-8} H).

Sensor Constants

Initially we tried to determine the sensor constants by optimizing Eq. [11] using all 14 nonconductive media. This resulted in a relatively high sum of squares for all the sensors. The poor fit was mainly due to the brasso and the sugar-water mixture with the highest amount of sugar, both of which had measured relative permittivities that were less than the calculated values. Excluding the brasso and the five sugar-water mixtures from the optimization improved the fit considerably. The lack of fit for the sugar-waters is not well understood. The fact that the fit is especially bad for the sugar-water with the highest amount of sugar (approaching saturation) suggests that the formation of sugar crystals might be the reason for the discrepancy. But this is only speculation at this time. Formation of sugar crystals on the dielectric probe, for example, will result in an underestimation of the measured permittivity. We have no explanation for the lack of fit for the brasso.

The sensor constants optimized using the remaining eight media are listed in Table 1. The comparison between the measured and calculated relative permittivities is excellent for all sensors (R^2 between 0.999 and 1.0). The values for the three optimized parameters show little variation between sensors. The stray capacitance C_s ranges from 9.75 to 10.47×10^{-12} F, the geometric factor for the medium g_m from 0.167 to 0.193 m, and the geometric factor for the plastic g_p from 0.616 to 0.653 m.

The fact that we find $g_m < g_p$, indicates that most of the electromagnetic field generated by the sensor remains confined to the access tube. Only a small portion of the field actually penetrates the surrounding medium. The presence of the access tube therefore clearly limits the measurement volume of the sensors. Note also that the values for C_s for Sensor 2.15 increased from 4.52×10^{-12} F for the simplified circuit to $10.18 \times$

Table 1. Optimized sensor constants.

Probe.sensor	C_s ($\times 10^{-12}$) F \dagger	g_m m	g_p m	R^2
1.1	9.84	0.193	0.625	0.999
1.2	9.97	0.172	0.634	0.999
1.3	10.25	0.168	0.620	1.000
1.4	10.22	0.167	0.619	1.000
1.5	10.18	0.175	0.626	1.000
1.6	10.23	0.176	0.618	1.000
1.7	10.16	0.179	0.636	1.000
1.8	9.96	0.182	0.631	0.999
1.9	10.15	0.175	0.624	1.000
1.10	10.41	0.174	0.619	1.000
1.11	10.39	0.169	0.627	1.000
1.12	10.11	0.172	0.635	1.000
1.13	10.13	0.170	0.619	1.000
1.14	10.12	0.174	0.641	1.000
2.1	10.17	0.170	0.639	1.000
2.2	10.13	0.176	0.629	1.000
2.3	10.03	0.184	0.631	1.000
2.4	10.28	0.176	0.619	1.000
2.5	10.34	0.182	0.625	1.000
2.6	10.38	0.175	0.637	1.000
2.7	10.32	0.182	0.621	1.000
2.8	9.75	0.188	0.619	1.000
2.9	9.98	0.180	0.616	1.000
2.10	10.17	0.174	0.619	1.000
2.11	10.16	0.174	0.619	1.000
2.12	10.26	0.170	0.622	1.000
2.13	10.47	0.170	0.618	1.000
2.14	10.45	0.175	0.635	1.000
2.15	10.18	0.177	0.653	1.000
Average	10.18	0.176	0.627	
SD	0.17	0.006	0.009	
Median	10.17	0.175	0.625	
Min	9.75	0.167	0.616	
Max	10.47	0.193	0.653	

\dagger Numbers in this column need to be multiplied by 10^{-12} .

10^{-12} F for the complete circuit. The increase in C_s is due to the different geometry. Additional stray capacitance is introduced with the brass electrode rings because some of the electric field goes directly from one electrode to the other through the plastic separation ring, thereby bypassing the access tube and the medium. It is unlikely that the capacitor C_c in the simplified circuit will contribute a significant amount of stray capacitance.

As an example, Fig. 3 shows the resonant frequency for Sensor 1.10 as a function of measured and optimized relative permittivity. The brasso and the five sugar-water mixtures are also shown, although they were ex-

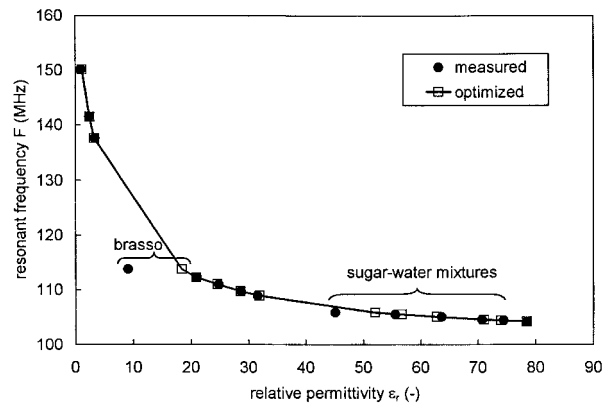


Fig. 3. Resonant frequency of Sensor 1.10 as a function of measured and optimized relative permittivity. The six data points representing the brasso and the sugar-water mixtures are not incorporated in the optimization.

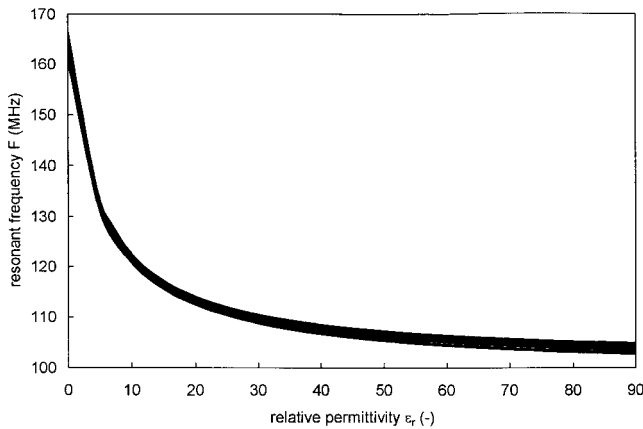


Fig. 4. Resonant frequency as a function of relative permittivity for all 29 sensors. Each curve is calculated by inserting the sensor constants of Table 1 into Eq. [4] (assuming no losses due to relaxation or conductivity).

cluded from the optimization. For the eight media that were included in the optimization, the model fits the data perfectly ($R^2 = 1.0$). Of the five sugar-waters that were excluded from the optimization, four also show a reasonable fit. As mentioned earlier, the relative permittivities of the brasso and the sugar-water mixture with the highest amount of sugar are overestimated by the fitted curve.

Finally, Fig. 4 shows the resonant frequency as a function of relative permittivity for all 29 sensors. Each curve is calculated by inserting the sensor constants of Table 1 into Eq. [4] (which assumes that there are no dielectric losses). Clearly, the frequency response of all sensors is very similar. The similarity of the response suggests that one set of constants may suffice to describe all sensors. This topic is discussed in more detail toward the end of this paper.

Ionic Conductivity

The effect of the medium's ionic conductivity on the frequency response of the sensors is discussed using data

from Sensor 1.10. The results for all the other sensors are similar. The relevant experimental data for Sensor 1.10 are given in Table 2. Note that the imaginary permittivity ϵ_r'' (determining the total dielectric losses) is the sum of the conductivity loss factor $\sigma\omega^{-1}\epsilon_0^{-1}$ and the relaxation loss factor $\epsilon_{r,rel}''$. Part of the variation in ϵ_r , ϵ_r'' , $\sigma\omega^{-1}\epsilon_0^{-1}$, and $\epsilon_{r,rel}''$ is due to the propanol-water and sugar-water mixtures is due not only to adding KCl but also to the experimental procedure. To increase the conductivity of the solutions, KCl was dissolved in pure water, and the resulting solution added to the mixtures. This procedure slightly altered the mixtures and therefore ϵ_r , ϵ_r'' , $\sigma\omega^{-1}\epsilon_0^{-1}$, and $\epsilon_{r,rel}''$. These alterations do not affect the analysis because ϵ_r , ϵ_r'' , and $\sigma\omega^{-1}\epsilon_0^{-1}$ are measured for each mixture while $\epsilon_{r,rel}''$ is calculated using Eq. [6].

The last three columns in Table 2 show that the effect of $\epsilon_{r,rel}''$ on ϵ_r'' is less pronounced than the effect of $\sigma\omega^{-1}\epsilon_0^{-1}$ (see also Eq. [6]). The ratio between $\sigma\omega^{-1}\epsilon_0^{-1}$ and $\epsilon_{r,rel}''$ is a measure of the importance of the conductivity effect over the relaxation effect. Except for the three lowest $\sigma\omega^{-1}\epsilon_0^{-1}$ values, this ratio is always higher than 1, and ranges from 1.5 to 41.0 (numbers not shown). The observed dominance of the conductivity effect over the relaxation effect on the total dielectric losses might not hold for soils. The interaction between soil water and soil particles is expected to increase the relaxation effect.

The measured and calculated frequency response of Sensor 1.10 is shown in Fig. 5. The calculated response is obtained by solving Eq. [11] for ω ($= 2\pi F$) using seven different levels of the loss factor G ($= g_m\omega\epsilon_r''\epsilon_0 = g_m\sigma + g_m\omega\epsilon_{r,rel}''\epsilon_0$). The figure illustrates the effect of dielectric losses on the sensor frequency. It does not allow for a direct comparison between measured and calculated values (this will be done further on). Note the change of scale on the y-axis as compared with the previous figures. The effect of dielectric losses on the frequency response is most pronounced for the medium with the lowest relative permittivity (propanol-water). Even a relatively small increase in G from 0.003 to 0.023 S

Table 2. Experimental data for studying the effect of the conductivity of the medium on the frequency response of Sensor 1.10.

Medium	Cond., σ	Freq., F	Rel. perm., ϵ_r	ϵ_r''	$\sigma\omega^{-1}\epsilon_0^{-1}$	$\epsilon_{r,rel}''$
	$S\ m^{-1}$	MHz				
Propanol-water						
1	0.000	108.99	31.55	2.91	0.00	2.91
2	0.036	108.23	32.98	7.95	5.93	2.02
3	0.066	107.54	33.74	14.63	10.98	3.64
4	0.113	106.28	34.47	22.66	19.18	3.48
5	0.192	104.58	36.49	38.67	33.05	5.62
6	0.294	103.24	38.74	58.17	51.19	6.98
Sugar-water						
1	0.001	105.24	61.23	4.85	0.17	4.68
2	0.040	105.09	60.75	11.48	6.84	4.64
3	0.084	104.76	62.21	20.17	14.36	5.80
4	0.126	104.40	62.78	30.67	21.61	9.06
5	0.160	104.16	62.38	33.75	27.65	6.10
6	0.197	103.94	62.53	40.15	34.09	6.06
7	0.296	103.14	63.36	58.72	51.59	7.13
Water						
1	0.001	104.31	78.46	1.65	0.10	1.54
2	0.033	104.35	78.01	6.35	5.62	0.73
3	0.047	104.33	77.96	8.69	8.12	0.57
4	0.090	104.18	78.18	17.42	15.53	1.90
5	0.144	103.97	78.39	26.89	24.91	1.98
6	0.294	103.19	78.42	52.53	51.28	1.25

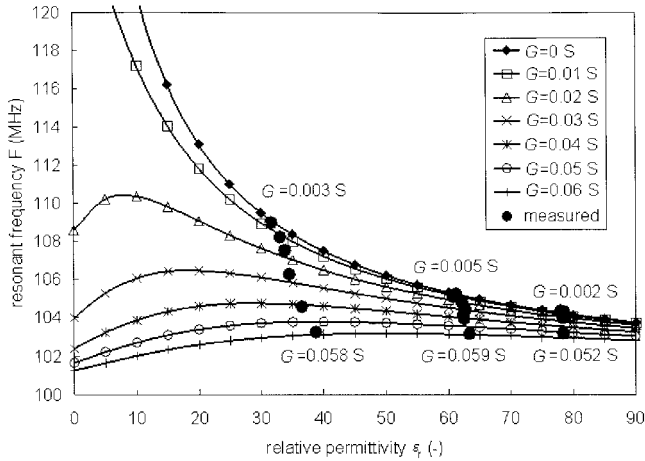


Fig. 5. Measured (dots) and calculated (lines plus symbols) resonant frequency as a function of relative permittivity for different levels of the dielectric losses expressed as G . The numbers in the figure show the range of G values for the propanol-water, the sugar-water, and the water. Results for Sensor 1.10.

for the propanol-water leads to a drop in frequency of 2.71 MHz. For propanol-water with $G = 0.023$ S, not accounting for dielectric losses would result in an overestimation of ϵ_r by 14.79 [= 49.26 (Eq. [4]) - 34.47].

Figure 5 also shows that for $G > 0.01$ S, the relationship between frequency and relative permittivity may no longer be unique. Different values of ϵ_r may result in the same sensor frequency. This is a serious problem as it implies that in soils with high conductivity or relaxation losses it may be impossible to relate the sensor frequency reading to the correct relative permittivity and therefore to the correct soil water content.

We checked whether this nonuniqueness problem might explain the odd behavior of brasso and the sugar-water mixture with the highest amount of sugar observed earlier. For Sensor 1.10, we found for brasso $F = 113.82$ MHz, $\epsilon_r = 9.088$, and $\epsilon_r'' = 2.719$ with a calculated G value of 0.003 S. For the sugar-water mixture we found $F = 105.87$ MHz, $\epsilon_r = 45.134$, and $\epsilon_r'' = 9.117$ with a calculated G value of 0.009 S. Solving Eq. [11] for C with the quadratic formula using the appropriate sensor constants for Sensor 1.10 (Table 1) results in $\epsilon_r = -10.41$ and $\epsilon_r = 18.35$ for brasso and in $\epsilon_r = -9.34$ and $\epsilon_r = 52.03$ for the sugar-water. This shows that the G values for both the brasso and the sugar-water are not high enough to result in two positive values for ϵ_r . Non-uniqueness is therefore not an issue for these two media, leaving us without a satisfactory explanation.

The effect of the dielectric losses on the sensor frequency is investigated further by plotting the sensor frequency for the propanol-water, the sugar-water, and the water as a function of G (Fig. 6). The bounding lines in the figure indicate the range of relative permittivities for each of these three media as calculated by the circuit model (Eq. [11] solved for ω). Figure 6 shows that the model describes the data reasonably well. Interestingly, at a G value of about 0.055 S, all three media generate about the same sensor frequency (103.2 MHz), despite the fact that their relative permittivities are significantly different (ranging from approximately 35 for

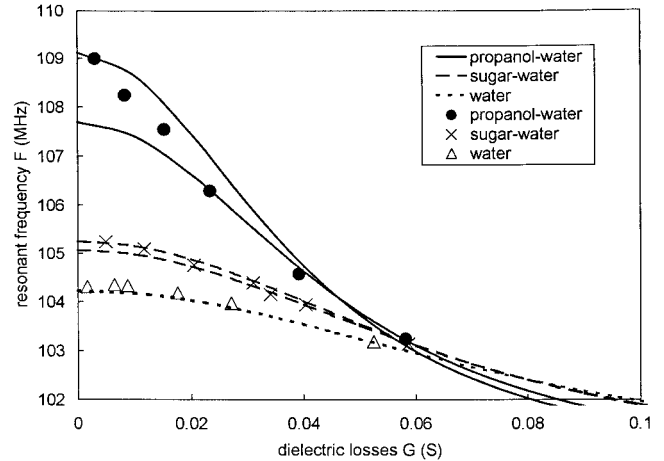


Fig. 6. Measured (symbols) and calculated (lines) resonant frequency as a function of the dielectric losses G for propanol-water, sugar-water, and water. Results for Sensor 1.10.

propanol-water to approximately 78 for water). This again shows that in lossy media, nonuniqueness problems are likely to occur if the relative permittivity is inferred from the sensor frequency alone.

The effectiveness of the model to compensate for dielectric losses can be evaluated by plotting the measured relative permittivity against the calculated relative permittivity (Fig. 7). Both the corrected data (solving Eq. [11] for C) and the uncorrected data (solving Eq. [4] for C) are shown. Results are given for Sensors 1.5, 1.10, 2.5, and 2.10. Note that for the corrected data two positive values for permittivity could often be calculated (nonuniqueness). In these cases, the smaller permittivity is plotted as an open circle, and the larger as a filled circle. The filled circles are in reasonably good agreement with the data, although significant deviations do occur. The deviations are most severe for the medium with the lowest permittivity (propanol-water) and for the media with the highest electrical conductivity. We showed earlier that failure to account for the effect of dielectric losses on the sensors (the uncorrected points) results in an overestimation of the relative permittivity. For Sensor 1.10, for example, Fig. 7 shows that the overestimation of ϵ_r may be as high as 67.7 for the propanol-water (measured ϵ_r between 32 and 39), 47.2 for the sugar-water (measured ϵ_r 61–63), and 30.1 for the water (measured ϵ_r 78).

The inability of the circuit model to accurately describe the media with low permittivity and high electrical conductivity is not due to the model itself but due to the unfortunate shape of the permittivity-frequency relationship at high G , a result of the sensor design. The higher the dielectric losses, the more the frequency becomes insensitive to the relative permittivity and the more the ϵ_r - F relationship approaches a horizontal line. Slight inaccuracies in the frequency or in the sensor constants may then result in serious errors in the calculated relative permittivity. For G values higher than those used in this study, the ϵ_r - F relationship will become completely horizontal. The frequency reading is then no longer influenced by the permittivity of the media. Or in other words, at high G , the dielectric losses

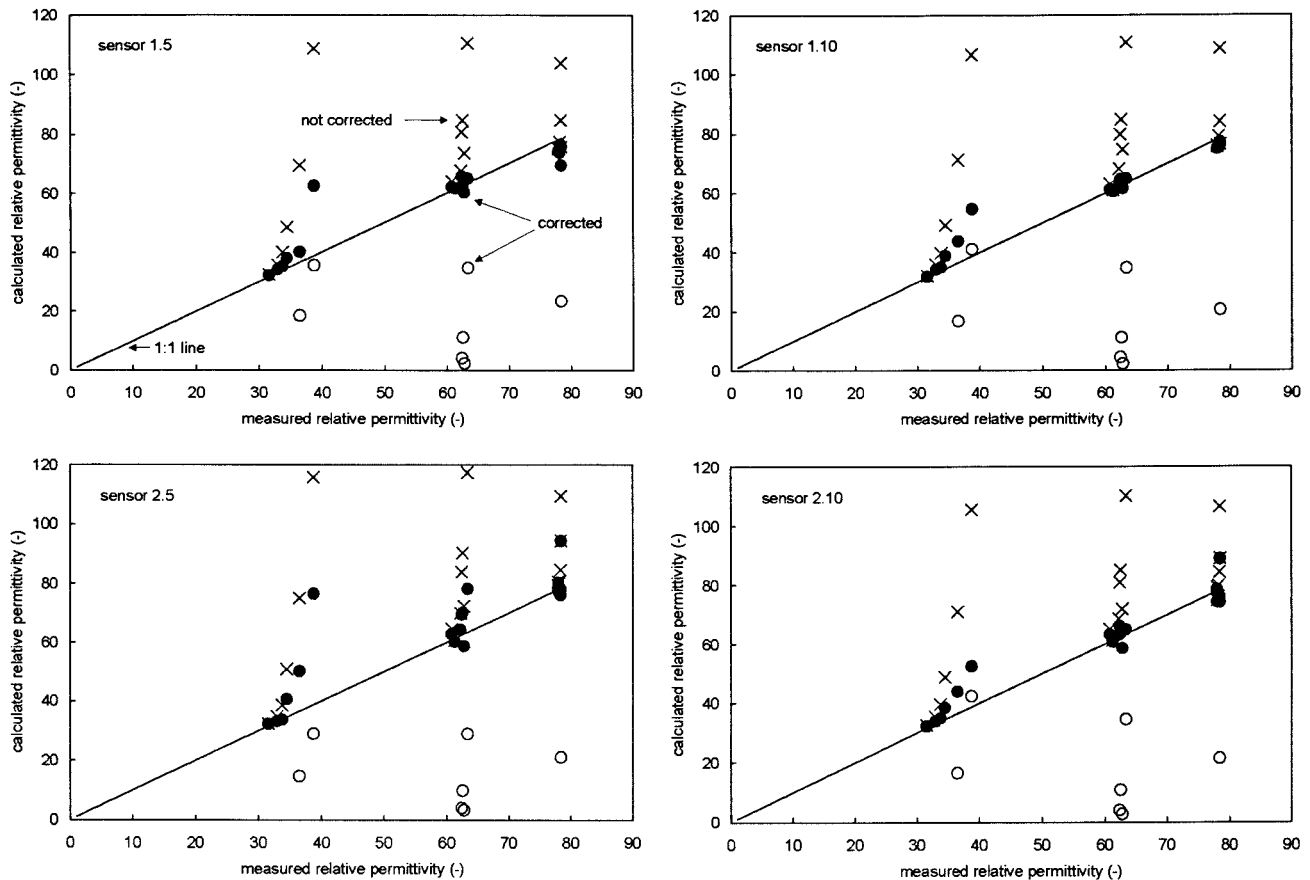


Fig. 7. Measured versus calculated relative permittivity. Both corrected data (dots, Eq. [11] solved for C) and uncorrected data (crosses, Eq. [4]) are shown. Results for Sensors 1.5, 1.10, 2.5, and 2.10.

are completely overshadowing the effect of the real permittivity on the sensor frequency.

A way of refining the circuit model might come from transmission line theory (Hilhorst, 1998). The two brass rings of the EnviroSCAN sensor can be considered as an open ended lossy transmission line. The electromagnetic properties of a unit length of transmission line are described by its characteristic impedance, Z_0 ($L^2 T^{-3} M I^{-2}$):

$$Z_0 = \sqrt{\frac{R_{s,1} + j\omega L_{s,1}}{G_1 + j\omega C_1}} \quad [14]$$

where R_s is the series resistance ($L^2 T^{-3} M I^{-2}$), L_s is the series inductance, G is the parallel conductance and C is the parallel capacitance. The subscript 1 is included to stress that the parameters in the equation are defined per unit length.

Incorporating the capacitance of the plastic access tube, C_p into Eq. [14] results in:

$$Z_0 = \sqrt{\frac{(R_{s,1} + j\omega L_{s,1})(j\omega C_1 + G_1 + j\omega C_{p,1})}{j\omega C_{p,1}(j\omega C_1 + G_1)}} \quad [15]$$

Note that C ($= g_m \epsilon_{r,m} \epsilon_0$), G ($= g_m \sigma + g_m \omega \epsilon_{r,rel}'' \epsilon_0$), and C_p ($= g_p \epsilon_{r,p} \epsilon_0$) were already included in our circuit model (Fig. 1). The factors R_s and L_s are new and describe the resistance losses and the storage of magnetic energy in the transmission line (brass rings), respectively. Hilhorst showed that it is possible to calculate the correct ϵ_r for

G values up to 0.1 S, by including R_s and L_s in a semi-empirical analysis of a sensor with two parallel electrodes. Incorporating Eq. [15] into our circuit model in a theoretically sound manner is hampered by the fact that the two brass rings do not constitute a uniform transmission line. Thus there is no straightforward method available to convert Z_0 into an impedance value Z for the rings. Considering the above, we think that the circuit model as presented in Fig. 1 remains the best available method to describe the frequency response of the EnviroSCAN sensor in lossy media.

Simplified Procedure for Sensor Calibration

Conventionally, for the Enviroscan sensor, differences in frequency response between sensors are corrected for by taking frequency measurements in air (F_a) and in water (F_w). The frequency measurement in the medium of interest (F_m) is then scaled, $SF = (F_a - F_m) / (F_a - F_w)$ (e.g., Paltineanu and Starr, 1997; Baumhardt et al., 2000). This normalization procedure becomes redundant if Eq. [11] is used to relate the sensor frequency to the permittivity of the medium. Equation [11], however, contains four unknown constants (C_s , L , g_m , and g_p). Frequency measurements in air and water alone do not suffice to determine these constants for each sensor. To avoid the need of using multiple media to calibrate each sensor (as is done in this study), we investigated

Table 3. Calculated sensor constants g_p and C_s for $g_m = 0.176$ m and $L = 9.38 \times 10^{-8}$ H. The R^2 values are obtained by using the shown constants to predict the relative permittivity of the eight nonconductive media in the original optimization process.

Probe.sensor	g_p	C_s	R^2
	m	($\times 10^{-12}$) F†	
1.1	0.605	10.41	0.999
1.2	0.621	10.20	0.999
1.3	0.610	10.37	0.999
1.4	0.611	10.28	0.999
1.5	0.615	10.37	1.000
1.6	0.608	10.44	1.000
1.7	0.625	10.41	1.000
1.8	0.617	10.29	0.999
1.9	0.613	10.36	1.000
1.10	0.610	10.57	1.000
1.11	0.618	10.49	1.000
1.12	0.625	10.27	0.999
1.13	0.613	10.21	1.000
1.14	0.631	10.30	1.000
2.1	0.630	10.28	0.999
2.2	0.620	10.32	1.000
2.3	0.618	10.37	1.000
2.4	0.609	10.47	1.000
2.5	0.614	10.63	1.000
2.6	0.629	10.54	1.000
2.7	0.610	10.58	1.000
2.8	0.606	10.12	1.000
2.9	0.606	10.24	1.000
2.10	0.610	10.35	1.000
2.11	0.610	10.31	1.000
2.12	0.613	10.39	1.000
2.13	0.610	10.59	1.000
2.14	0.625	10.64	1.000
2.15	0.642	10.42	1.000
Average	0.616	10.39	
SD	0.009	0.13	
Median	0.613	10.37	
Min	0.605	10.12	
Max	0.642	10.64	

† Numbers in this column need to be multiplied by 10^{-12} .

whether it is possible to fix two of the constants based on the results obtained so far, and to calculate the other two based on F_a and F_w .

In the simplified approach, the value of L remains fixed at 9.38×10^{-8} H (consistent with the approach discussed earlier). From a theoretical standpoint, C_s should not be fixed as this parameter describes the stray capacitance in the electrical circuit and is likely to vary between sensors. This leaves us with the choice of either fixing g_m or g_p . Trial calculations showed that fixing g_m gives much better results than fixing g_p (highest R^2 when the new constants are used to calculate the permittivity for the eight nonconductive media with Eq. [11]). If g_m is fixed, the capacitances of the media only depend on the calculated relative permittivities, resulting in appropriate values for g_p and C_s . In contrast, if g_m is not fixed, the capacitances of the media change both with g_m and the calculated relative permittivity, resulting in a good fit for the air and water, but also resulting in potentially inappropriate values for g_p and C_s (and a potentially bad fit for the other six nonconductive media).

Based on this information we choose to fix L to 9.38×10^{-8} H, fix g_m to 0.176 m (the average value in Table 1), and calculate g_p ($= C_p/\epsilon_r \epsilon_0$) and C_s . Calculations were conducted by solving Eq. [4] using ($F_a, \epsilon_r = 1$) and ($F_w, \epsilon_r = 78.54$). We preferred Eq. [4] to the more general Eq. [11] because Eq. [4] results in a relatively simple analytical solution. Use of Eq. [4] implies that relaxation

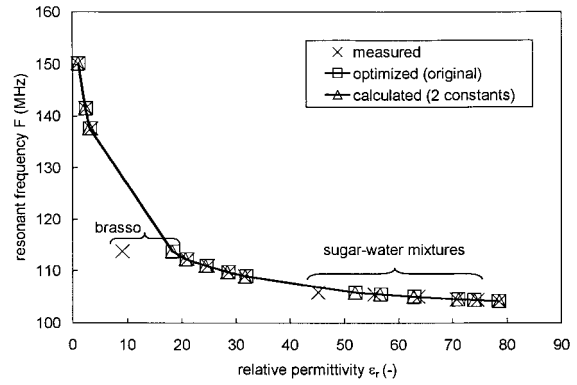


Fig. 8. Resonant frequency of Sensor 1.10 as a function of measured, optimized, and calculated relative permittivity. The six data points representing the brasso and the sugar-water mixtures are not incorporated in the optimization.

losses in the water are neglected. It also means that di-water must be used for measuring F_w because ionic conductivity losses are not accounted for. The calculated values for g_p and C_s are shown in Table 3. The R^2 values of between 0.999 and 1.000 show that the fit between measured and calculated permittivity for the eight nonconductive fluids are excellent with the new sensor constants.

Calculated values for g_p vary from 0.605 to 0.642 m and for C_s from 10.12×10^{-12} to 10.64×10^{-12} F. Comparing Tables 1 and 3 shows that fixing g_m results in a slight decrease in the value of g_p and a slight increase in the value of C_s for all the sensors. As an example, Fig. 8 shows the resonant frequency of Sensor 1.10 as a function of measured, optimized (Table 1), and calculated (Table 3) relative permittivity. Again disregarding the brasso and the five sugar-water mixtures, the fit is excellent for the simplified procedure.

We also tested the effect of using the average constants in Table 1 for all the sensors. This resulted in a decrease in the goodness of fit for some sensors (R^2 values for the eight nonconductive media ranging from 0.988 to 1.000) and is therefore not advised. For example, for the sensor with the worst fit (Sensor 2.15, $R^2 = 0.988$), the calculated relative permittivity for water was 111.84 against a measured value of 78.54. This shows that significant errors might occur when average constants are used to calculate permittivity, despite the high R^2 values. The use of one particular set of constants (Sensor 1.10) for all the other sensors was also tested. This also yielded a decrease in the goodness of fit for some sensors (R^2 between 0.989 and 1.000). From these results we conclude that some kind of normalization procedure remains necessary. There is not one set of constants that describes the behavior of all the sensors.

Capacitance Probe Sensors in Soil

The results of this study indicate that in nonlossy materials there is a clear relationship between the resonant frequency of the capacitance probe sensors and the permittivity of the medium. Applying the sensors in coarse and medium textured soils with low electrical conductivity should therefore give an accurate estimate

of the soil permittivity and hence of the soil water content. However, applying capacitance probe sensors in fine textured soils or in saline soils might be problematic due to complications associated with high dielectric losses. Fine textured soils might generate high dielectric losses due to the presence of bound water with a relatively low relaxation frequency. Saline soils might result in high dielectric losses due to ionic conductivity.

High dielectric losses influence the frequency-permittivity relationship for the sensors in three different ways. First, it may prove impossible to relate the measured resonant frequency to the correct permittivity of the soil and hence to the correct soil water content because of nonuniqueness of the frequency-permittivity relationship in lossy media. Second, in saline soils, the sensor frequency may respond more to changes in soil salinity than to changes in soil water content because the frequency becomes insensitive to permittivity when ionic conductivity is high. And third, the susceptibility of the frequency to ionic conductivity implies that the sensor is also sensitive to soil temperature (conductivity in a saline soil changes as a function of soil temperature).

The performance of capacitance probe sensors in saline soils might be improved by increasing the frequency of operation of the sensors. The higher the frequency, the lower the $\sigma\omega^{-1}\epsilon_0^{-1}$ term, and the lower the dielectric losses G . However, the frequency of operation cannot be increased too much because it should remain below the relaxation frequency of the soil water.

CONCLUSIONS

The electric circuit model proved partially successful in describing the relationship between sensor frequency and medium permittivity for 29 EnviroSCAN capacitance probe sensors. Six of the 14 media had to be excluded from the optimization to obtain good agreement between the model and the data. The lack of fit for the five sugar-waters might have been the result of the formation of sugar crystals that affected the measurements of the complex permittivity. The lack of agreement for the brasso could not be explained. The four optimized constants in the circuit model were unique for each sensor and varied within narrow limits between sensors.

We found a profound influence of ionic conductivity on the sensor resonant frequency. The higher the conductivity of the medium, the lower the sensor frequency. The effect was most pronounced for the medium with the lowest relative permittivity (propanol-water). The effect of ionic conductivity on the sensors was generally more significant than the effect of relaxation losses. The circuit model did a good job in correcting for the conductivity effects. As the dielectric losses increased however, the frequency became insensitive to permittivity and small inaccuracies in the measured frequency or in the sensor constants resulted in large errors in the calculated permittivity. The circuit model might be refined further by using transmission line theory to describe the electromagnetic properties of the sensor's brass rings in more detail.

A satisfactory simplified calibration procedure consisted of fixing the sensor constants L to 9.38×10^{-8} H and g_m to 0.176 m, and calculating the constants g_p and C_s using sensor readings in air and water. The error introduced by not optimizing all four constants was small (the R^2 for the calculated permittivity of the eight nonconductive media was 0.999–1.000 for all sensors). The use of one set of sensor constants for all sensors was not recommended because the R^2 for individual sensors became as low as 0.988.

APPENDIX: EQUATION [11] SOLVED FOR ANGULAR FREQUENCY AND MEDIUM CAPACITANCE

Equation [11] solved for angular frequency results in:

$$\omega = \sqrt{\frac{-b \pm \sqrt{b^2 - 4ac}}{2a}} \quad [A1]$$

with:

$$\begin{aligned} a &= -C_s LC_p^2 - 2C_s LC_p C - C_s LC^2 - LC_p^2 C - LC_p C^2 \\ b &= C_p^2 + 2C_p C + C^2 - C_s LG^2 - LC_p G^2 \\ c &= G^2 \end{aligned}$$

Equation [11] solved for medium capacitance results in:

$$C = \frac{-b \pm \sqrt{b^2 - 4ac}}{2a} \quad [A2]$$

with:

$$\begin{aligned} a &= \omega^2 - \omega^4 C_s L - \omega^4 LC_p \\ b &= 2\omega^2 C_p - 2\omega^4 C_s LC_p - \omega^4 LC_p^2 \\ c &= \omega^2 C_p^2 + G^2 - \omega^4 C_s LC_p^2 - \omega^2 C_s LG^2 - \omega^2 LC_p G^2 \end{aligned}$$

The appropriate sign in front of the square root of the discriminant in Eq. [A1] is always a minus. In Eq. [A2] the appropriate sign is a minus if the dielectric losses G are low. However, at high G , a plus sign may also result in positive values for C in Eq. [A2] (non-uniqueness).

ACKNOWLEDGMENTS

The authors thank Tom Pflaum (USDA-ARS, Parlier) for helping to select the fluids, Richard Austin (USDA-ARS, Riverside) for assistance during the capacitor experiments, and Inma Lebron (USDA-ARS, Riverside) for allowing us to use her laboratory. This work was supported in part by USDA NRI grant 2002-35107-12507 (David Robinson) and by the SAHRA science and technology center under NSF grant EAR-9876800 (Marcel Schaap).

REFERENCES

- Baker, J.M., and R.R. Allmaras. 1990. System for automating and multiplexing soil moisture measurement by time-domain reflectometry. *Soil Sci. Soc. Am. J.* 54:1–6.
- Baumhardt, R.L., R.J. Lascano, and S.R. Evett. 2000. Soil material, temperature, and salinity effects on calibration of multisensor capacitance probes. *Soil Sci. Soc. Am. J.* 64:1940–1946.
- Bell, J.P., T.J. Dean, and M.G. Hodnett. 1987. Soil moisture measure-

- ment by an improved capacitance technique, part II. Field techniques, evaluation and calibration. *J. Hydrol. (Amsterdam)* 93:79–90.
- Coleman, T.F., M.A. Branch, and A. Grace. 1999. Optimization toolbox for use with Matlab. The MathWorks Inc., Natick, MA.
- Dean, T.J. 1994. The IH capacitance probe for measurement of soil water content. Rep. No. 125, Institute of Hydrology, Wallingford, UK.
- Dean, T.J., J.P. Bell, and A.J.B. Baty. 1987. Soil moisture measurement by an improved capacitance technique, part I. Sensor design and performance. *J. Hydrol. (Amsterdam)* 93:67–78.
- Dirksen, C., and S. Dasberg. 1993. Improved calibration of time domain reflectometry soil water content measurements. *Soil Sci. Soc. Am. J.* 57:660–667.
- Dobson, M.C., F.T. Ulaby, M.T. Hallikainen, and M.A. El-Rayes. 1985. Microwave dielectric behavior of wet soil. Part II: Dielectric mixing models. *IEEE Trans. Geosci. Remote Sens* GE-23:35–46.
- Evelt, S.R., and J.L. Steiner. 1995. Precision of neutron scattering and capacitance type soil water content gauges from field calibration. *Soil Sci. Soc. Am. J.* 59:961–968.
- Fellner-Felldg, H. 1969. The measurement of dielectrics in the time domain. *J. Phys. Chem.* 73:616–623.
- Friedman, S.P. 1998. A saturation degree-dependent composite spheres model for describing the effective dielectric constant of unsaturated porous media. *Water Resour. Res.* 34:2949–2961.
- Gardner, C.M.K., D.A. Robinson, K. Blyth, and J.D. Cooper. 2000. Soil water content. p.1–64. *In* K.A. Smith, and C.E. Mullins (ed.) *Soil and environmental analysis: Physical methods*. Marcel Dekker, New York.
- Heimovaara, T.J. 1994. Frequency domain analysis of time domain reflectometry waveforms. 1. Measurement of the complex dielectric permittivity of soils. *Water Resour. Res.* 30:189–199.
- Heimovaara, T.J., E.J.G. de Winter, W.K.P. van Loon, and D.C. Esveld. 1996. Frequency-dependent dielectric permittivity from 0 to 1 GHz: Time domain reflectometry measurements compared with frequency domain network analyzer measurements. *Water Resour. Res.* 32:3603–3610.
- Hilhorst, M.A. 1998. Dielectric characterization of soil. Ph.D. diss. Wageningen Agric. Univ., Wageningen, The Netherlands.
- Kraus, J.D. 1984. *Electromagnetics*. Third ed. McGraw-Hill, New York.
- Malicki, M.A., R. Plagge, and C.H. Roth. 1996. Improving the calibration of dielectric TDR soil moisture determination taking into account the solid soil. *Eur. J. Soil Sci.* 47:357–366.
- Mead, R.M., J.E. Ayars, and J. Liu. 1995. Evaluating the influence of soil texture, bulk density and soil water salinity on a capacitance probe calibration. ASAE Paper 95–3264. ASAE, St. Joseph, MI.
- Morgan, K.T., L.R. Parsons, T.A. Wheaton, D.J. Pitts, and T.A. Obreza. 1999. Field calibration of a capacitance water content probe in fine sand soils. *Soil Sci. Soc. Am. J.* 63:987–989.
- Noborio, K. 2001. Measurement of soil water content and electrical conductivity by time domain reflectometry: A review. *Comput. Electron. Agric.* 31:213–237.
- Paltineanu, I.C., and J.L. Starr. 1997. Real-time soil water dynamics using multisensor capacitance probes: Laboratory calibration. *Soil Sci. Soc. Am. J.* 61:1576–1585.
- Robinson, D.A., C.M.K. Gardner, J. Evans, J.D. Cooper, M.G. Hodnett, and J.P. Bell. 1998. The dielectric calibration of capacitance probes for soil hydrology using an oscillation frequency response model. *Hydrol. Earth Syst. Sci.* 2:111–120.
- Terman, F.E. 1943. *Radio engineers' handbook*. First ed. McGraw-Hill, New York.
- Topp, G.C., J.L. Davis, and A.P. Annan. 1980. Electromagnetic determination of soil water content: Measurements in coaxial transmission lines. *Water Resour. Res.* 16:574–582.
- Von Hippel, A.R. 1954. *Dielectric materials and applications*. John Wiley & Sons, New York.